Mechanistic principles of nanoparticle evolution to zeolite crystals

TRACY M. DAVIS[1], TIMOTHY O. DREWS[1], HARIKRISHNAN RAMANAN[1,2], CHUAN HE[1], JINGSHAN DONG[1], HEIMO SCHNABLEGGER[3], MARKOS A. KATSOULAKIS[4], EFROSINI KOKKOLI[1], ALON V. MCCORMICK[1], R. LEE PENN[2] AND MICHAEL TSAPATSIS[1]*

[1]University of Minnesota, Department of Chemical Engineering and Materials Science, 151 Amundson Hall, 421 Washington Avenue SE, Minneapolis, Minnesota 55455, USA
[2]University of Minnesota, Department of Chemistry, B-4, 139 Smith Hall, 207 Pleasant Street SE, Minneapolis, Minnesota 55455, USA
[3]Anton Paar GmbH, Anton-Paar-Str. 20, A-8054 Graz, Austria
[4]University of Massachusetts, Department of Mathematics and Statistics, 710 North Pleasant Street, Amherst, Massachusetts 01003, USA
*e-mail: tsapatsi@cems.umn.edu

Published online: 16 April 2006; doi:10.1038/nmat1636

Precursor nanoparticles that form spontaneously on hydrolysis of tetraethylorthosilicate in aqueous solutions of tetrapropylammonium (TPA) hydroxide evolve to TPA-silicalite-1, a molecular-sieve crystal that serves as a model for the self-assembly of porous inorganic materials in the presence of organic structure-directing agents. The structure and role of these nanoparticles are of practical significance for the fabrication of hierarchically ordered porous materials and molecular-sieve films, but still remain elusive. Here we show experimental findings of nanoparticle and crystal evolution during room-temperature ageing of the aqueous suspensions that suggest growth by aggregation of nanoparticles. A kinetic mechanism suggests that the precursor nanoparticle population is distributed, and that the 5-nm building units contributing most to aggregation only exist as an intermediate small fraction. The proposed oriented-aggregation mechanism should lead to strategies for isolating or enhancing the concentration of crystal-like nanoparticles.

The structure of nanoparticles present in tetrapropylammonium (TPA)–silica sols made from tetraethylorthosilicate (TEOS), tetrapropylammonium hydroxide (TPAOH), and water, and their role (spectators versus participants) in nucleation and growth of TPA-silicalite-1 (referred to as silicalite-1 from here on) is a subject of considerable fundamental and practical significance[1–10]. Of fundamental importance is the relationship of these nanoparticles to the nuclei and building units of silicalite-1, an all-silica zeolite prototype for templated crystal growth. The potential to control nucleation and growth of preferentially oriented zeolite thin films[11] and to tailor zeolite crystal size and shape[12] makes studying the evolution of nanoparticles in TPA-silica sols a worthwhile endeavour.

Several hypotheses regarding the nature of the spontaneously formed nanoparticles and their role, or lack thereof, in the formation of silicalite-1 have been proposed. According to one hypothesis, the nanoparticles are colloidally stable, amorphous species that do not directly participate in the growth of silicalite-1, but serve as a source of nutrients during crystal growth[13]. Another hypothesis states that precursor nanoparticles contribute to growth, and their addition to the growing crystal can be rate limiting[14]. A third hypothesis is that the nanoparticles not only contribute to growth by direct addition, but also possess the silicalite-1 crystal structure[15]. Motivated by earlier reports that indicated zeolite crystal formation at room temperature both from clear sols[2] and from precipitated silica[16], we followed the evolution of nanoparticles at ambient conditions for more than one year by small-angle X-ray scattering (SAXS), high-resolution transmission electron microscopy (HRTEM), *in situ* atomic force microscopy (AFM) and cryogenic transmission electron microscopy (cryo-TEM) up to and beyond silicalite-1 crystal formation. The room-temperature study eliminated potential complications that may originate when quenching high-temperature experiments for

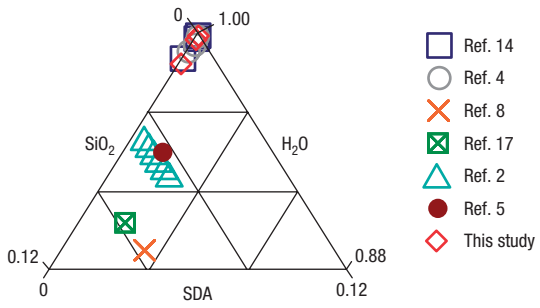

Figure 1 Composition space. Sampling of the composition (molar fraction) space investigated in previous TPA-silicalite-1 growth studies compared with those explored in this study.

characterization. Such complications can easily be foreseen on the basis of the temperature dependence of silica solubility and the dynamic nature of the precursor nanoparticles. In addition to establishing conclusively that the precursor nanoparticles are a metastable phase at room temperature, the slow transformation allowed, for the first time, isolation, purification and imaging of zeolite crystals at the initial stages of formation (that is, zeolite yield less than 5%). A new mechanism for aggregative crystal growth, and a mathematical model formulated according to this mechanism will be presented and shown to be in agreement with the experimental findings. According to the proposed mechanism, the metastable precursor nanoparticles, although not having the silicalite-1 structure, are found to participate in crystal growth by directly adding to the growing crystal after a certain stage in their evolution.

Figure 1 shows the composition space investigated here along with those used in other related silicalite-1 growth studies from clear sols[2,4,5,8,14,17]. The compositions used in this study are relatively dilute in TPAOH and TEOS and are similar to the ones used in other recent investigations[4,14]. More specifically, we report on experiments carried out using the following compositions

5 SiO_2:9 TPAOH:8,100 H_2O:20 EtOH (noted as C1)

20 SiO_2:9 TPAOH:8,100 H_2O:80 EtOH (noted as C3)

120 SiO_2:9 TPAOH:8,100 H_2O:480 EtOH (noted as C8).

At compositions comparable to C1, most of the silica added is present in the form of dissolved monomeric species ($Si(OH)_4$ and $Si(OH)_3O^-$), that is, no nanoparticles can be detected by SAXS. The absence of nanoparticles at compositions comparable to C1 was previously confirmed by means of dynamic light scattering (DLS)[14], and was also verified by our own SAXS and cryo-TEM measurements. Moreover, no growth or dissolution of silicalite-1 was observed for seeded-growth experiments carried out at similar compositions and temperatures between 60 and 90 °C, indicating that silicalite-1 can coexist in equilibrium with C1[14].

At C3 to C8, nanoparticles are evident by SAXS, in agreement with previous SAXS and DLS reports[4,14]. For seeded-growth experiments at compositions C3 to C8, silicalite-1 growth takes place with an apparent activation energy of 90 kJ mol^{-1}, and a growth rate that is nearly independent of composition[14]. Using DLVO theory[14], it has been shown that the apparent activation energy for seeded crystal growth is consistent with the idea that the rate-limiting step is the addition of nanoparticles to the growing seed crystal. It was suggested that nanoparticle rearrangements, if they occur, may take place on a timescale shorter than that of nanoparticle attachment. The particles were assumed to be spherical and to possess a surface potential similar to silicalite-1, however, no conclusion could be made regarding their structure, that is, amorphous versus silicalite-1 fragment or intermediate. It was also noted that use of the entire particle population (10^{17} particles cm^{-3}) resulted in over predicting the growth rate, indicating that only a fraction of the nanoparticles contribute to crystal growth.

Figure 2 shows SAXS and cryo-TEM characterization of the precursor nanoparticles before the appearance of silicalite-1 crystals. Figure 2a shows representative SAXS patterns of intensity versus $q = (4\pi/\lambda)\sin\theta$, where θ is half the scattering angle and λ is the wavelength of the incident beam, obtained from C3 during an ageing period of 196 days at room temperature. The data show increasing scattering intensity with increasing time at room temperature. There is a relatively rapid intensity increase in the first 22 days, followed by a slower intensity increase from day 22 to about day 70. The rate of intensity increase is reduced further from day 70 to day 196. The scattering data was transformed into pair-distance distribution functions (PDDF) (see Fig. 2b) using the generalized indirect Fourier transform (GIFT) software[18,19]. The PDDF (Fig. 2b) show that during the first 196-day period, a single population of spherical particles exists. To determine the average particle radius and polydispersity, the experimental PDDF were fitted by a Schultz distribution of spheres[20,21]. Figure 2c shows the evolution of the average nanoparticle radius, r_{avg}, and the error bars represent one standard deviation of r_{avg}. The average particle size increases rapidly during the first 22 days of ageing, continues to increase until day 100, and then remains nearly constant for the remaining time. In addition, small-angle neutron scattering (SANS) measurements confirmed that the nanoparticles possess a (silica rich) core-(TPA rich) shell structure that is preserved at least up to 150 days at room temperature (see Supplementary Information, Fig. S1). Although it is possible that there is initially TPA present in the interior (core) of the precursor nanoparticles (or a fraction thereof) and silica present in the shell, we will adopt the postulate that all precursor nanoparticles consist initially of a silica core and a TPA shell[4]. The SAXS and SANS data provide no evidence to support the presence of precursor nanoparticles with the silicalite-1 structure (for example, nanoslabs)[15].

In addition, the SAXS data are in agreement with the cryo-TEM images of the precursor nanoparticles shown in Fig. 2d,e. The images show spherical particles that increase in size during ageing. The sizes estimated from TEM are in good agreement with the SAXS sizes shown in Fig. 2c.

The ratio of absolute SAXS intensity[22] at $q = 0$, $I^{abs}_{sample}(q = 0)$, over the square of the particle volume, V (see Supplementary Information, Equation (HH)), is plotted as a function of time in Fig. 2c. The ratio decreases during the first ~100-day period of nanoparticle evolution and then remains constant. For $I^{abs}_{sample}(q = 0)/V^2$ to remain constant, any change in the number of nanoparticles should be exactly counter-balanced by a change in the square of the contrast between nanoparticles and the surrounding medium, or both the contrast and the number concentration should remain fixed during this time. In the absence of any evidence for the former, the latter scenario is adopted. The presence of a prolonged nucleation stage, where the size and number of precursor nanoparticles remains constant, followed by the room-temperature transformation to zeolite crystals indicates that the precursor nanoparticles exhibit metastability as was suggested by recent simulations[23].

Analysis of the SAXS and cryo-TEM data taken collectively is consistent with an initial evolution in particle size and number followed by an extended period where the majority of the particles remain unchanged in size and number. During the second stage,

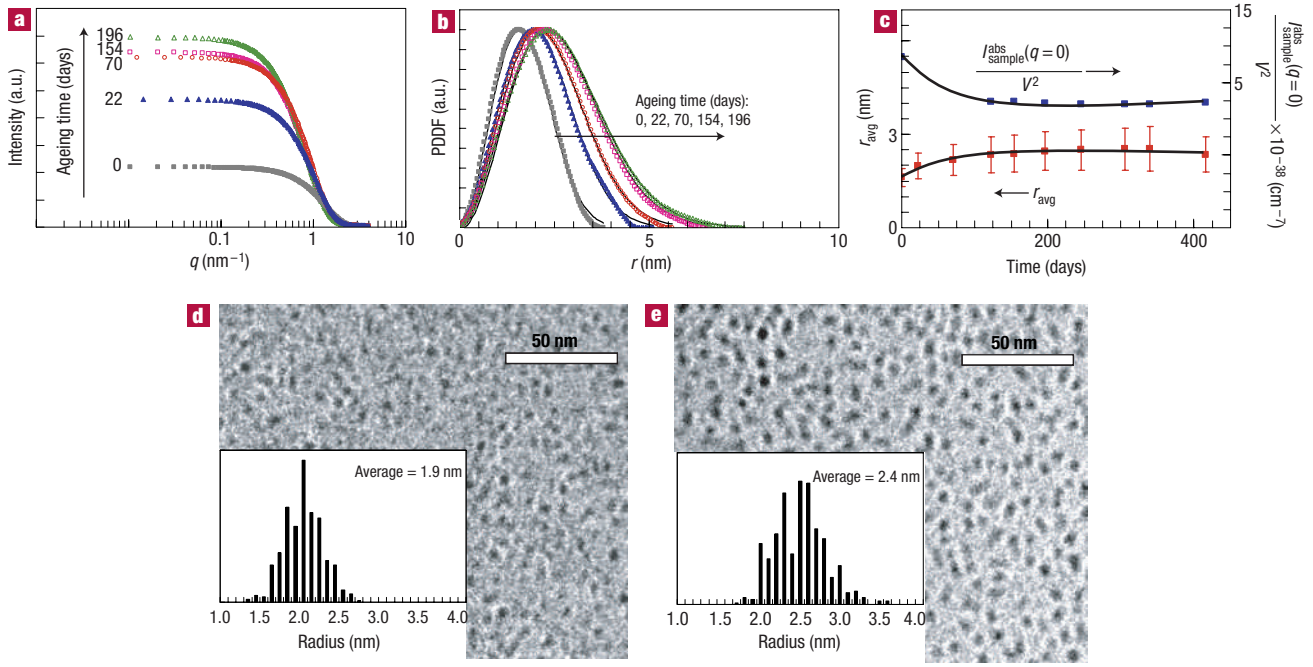

Figure 2 Characterization of precursor nanoparticles from C3. a, SAXS intensity profiles from precursor nanoparticles for ageing at room temperature up to day 196. **b**, Corresponding PDDF of the C3 intensity profiles shown in **a**. The symbols give PDDF determined from experimental data by use of the GIFT software. The lines are the corresponding PDDF fits of a Schultz distribution of spheres (see the Supplementary Information). **c**, The average precursor nanoparticle radius (red squares) and the intensity to size ratio (blue squares) are shown as a function of time. The error bars for the nanoparticle radii indicate the r_{avg} standard deviation of the corresponding Schultz distributions of spheres shown in **b**. Precursor nanoparticle sizes beyond 200 days are from the SAXS data presented in Fig. 3. **d**, Cryo-TEM image of fresh nanoparticles with particle size distribution (inset). **e**, Cryo-TEM image of 180-day aged nanoparticles with particle size distribution (inset).

changes to the composition of the precursor nanoparticles cannot be excluded if limited to an exchange of TPA for water molecules in the particles. Such compositional changes can occur without detection by SAXS because water and TPA have similar contrast (by X-rays).

After 245 days of ageing, a second population, characterized by a much larger particle size, emerges. Before this, no evidence for the existence of larger particles was observed by SAXS or TEM. Figure 3a shows SAXS profiles up to day 339. The relatively sharp increase in the low-q scattering intensity indicates the second population, and X-ray diffraction (XRD) analysis showed that these particles are silicalite-1 crystals (see Supplementary Information, Fig. S2). TEM analysis confirmed this finding, and revealed remarkable morphological characteristics that will be described in detail later.

The silicalite-1 crystals continue to grow relatively slowly (growth rate ~0.2 nm per day) as indicated by SAXS, HRTEM, DLS and scanning electron microscopy (SEM) measurements at subsequent ageing times. Figure 3b shows the evolution of the silicalite-1 crystal radius, along with the precursor nanoparticle size evolution during this experiment. The long time (~200 days) for nucleation of these crystals at room temperature is evident. Furthermore, the measured growth rate at room temperature is in agreement with the previously reported[14] seeded-growth data at a similar composition and elevated temperatures, and with the reported activation energy of 90 kJ mol^{-1} (see Supplementary Information, Fig. S3) indicating a similar crystal growth mechanism.

Isolation of the silicalite-1 crystals by dialysis permitted further analysis by TEM. This dialysis procedure allows unaltered crystals to be suspended in water nearly free of other forms of silica (precursor nanoparticles or dissolved species) and TPA ions. Samples can then be prepared for TEM observation free of artefacts caused by silica and TPA precipitation on water evaporation. SAXS analysis (see Supplementary Information, Fig. S4) indicated that the crystals are not affected significantly by the dialysis procedure, whereas the precursor nanoparticles are dissolved.

TEM (Fig. 4a) revealed crystals with radii up to 50 nm at day 305 when the crystal yield is low (less than 5%). Crystal size of 50 nm was verified using XRD line widths and the Scherrer equation. The crystal size is similar to that obtained at much higher crystal yields. This finding, that large crystals are obtained at low yields, is rather remarkable and should be accounted for in any proposed crystal growth mechanism. TEM images at higher magnification (Fig. 4b and Supplementary Information, Fig. S5), show a crystal morphology that is not well developed. The crystals can be described as aggregate-like clusters of oriented nanocrystalline domains (about 5 nm). Void spaces formed between the crystalline domains extend over the length scale of the cluster and are evenly distributed. The size of the crystalline domains is equal to the size of the nanoparticles determined by SAXS. Such near-single-crystalline, aggregate-like crystals with domains of the order of the precursor nanoparticles are indicative of crystal growth by oriented aggregation[14,24–30]. To our knowledge, similar nanostructures have not been observed in zeolite crystals grown slowly from precursor nanoparticles in the absence of a gel or precipitate. Furthermore, the crystals observed in the present study are very different from the compact morphologies reported for the aluminosilicate zeolites faujasite (FAU) and A (LTA) in systems for which a gel to zeolite transformation has been proposed[31,32]. These

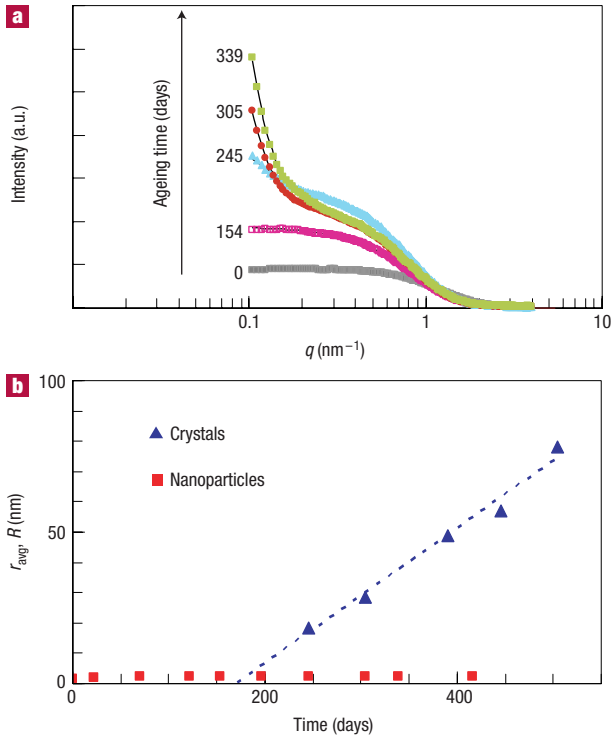

Figure 3 Emergence and evolution of silicalite-1 crystals in C3. a, SAXS measurements for ageing at room temperature up to 339 days. After 245 days, along with the precursor nanoparticles, a second population emerges, which is shown to be silicalite-1 by XRD (see Supplementary Information, Fig. S2) and TEM (see Fig. 4). **b**, Evolution of the precursor nanoparticle (squares from Fig. 2b) and TPA-silicalite-1 crystal radius (triangles). All radii were determined by SAXS except for some of the TPA-silicalite-1 radii, which, after 350 days, were measured by DLS and SEM. The linear crystal growth rate of the crystals, as determined by a least-squares fit (dotted line) to the experimental data (triangles), is 0.2 nm per day.

crystals are also different from the compact crystals of silicalite-1 formed at higher temperature and higher yields[33].

Further examination of the silicalite-1 crystals by HRTEM permitted a detailed analysis of the aggregate-like structure. An HRTEM view down the *b* axis of silicalite-1 is shown in Fig. 4c and Supplementary Information, Fig. S6. The images reveal that the aggregate-like clusters are single crystals with slightly misoriented domains. To illustrate the misorientation (see Fig. 4c), a set of parallel lines are drawn. The line in domain A is parallel to the ⟨101⟩ plane, whereas in domain B, the parallel line is slightly tilted with respect to the ⟨101⟩ plane. Similar misorientations are evident in other domains of the crystal as well. This type of misorientation has been documented[30] in other nanocrystalline materials that grow through oriented attachment.

The aggregate-like morphology of the silicalite-1 crystals formed at room temperature and concentration C3 is the strongest direct evidence that the nanoparticles actively participate in the nucleation and crystallization processes. The aggregate-like morphology cannot be explained by diffusion-limited growth from monomeric silica and TPA alone, considering the characteristically short times for diffusion of these species compared with the characteristically long times for crystal growth. More specifically, the time required for a silicalite-1 crystal to grow by 1 nm at room temperature and composition C3 is of the order of a day. Using the diffusivity for dissolved silica of 1.0×10^{-5} cm^2 s^{-1} (ref. 34), the characteristic time for diffusion over 1 μm is a fraction of a minute. Accordingly, the monomeric silica (and similarly TPA) concentration should be uniform around and in the pore space of the growing crystals, and thus diffusion-limited growth from this mobile species can be excluded under these conditions. Alternative growth models involving monomeric silica addition with the crystal growth rate controlled by the desorption of TPA from the nanoparticle exterior are also unlikely. Such a process would require the opening of sites for monomeric silica attachment, followed by surface poisoning in a rhythmic fashion every 5 nm. Even if such a process was possible, the persistence of empty spaces throughout the particle could not be accounted for by monomer addition considering the fast diffusion of these species.

Following the initial stages of crystal growth, more compact crystals appear. At 80% yield (504 days), typical pill-shaped 100-nm silicalite-1 crystals are obtained, indicating that Ostwald ripening and growth by monomer addition are at play. These competing rate processes, although insignificant during the early stages of growth, become important later due to the increased surface area of the crystals, the increased pH associated with silicalite-1 formation, and the reduced nanoparticle concentration.

Additional insight into the nanoparticles' role in silicalite-1 formation can be gained by studying crystal growth in the absence of detectable nanoparticles, that is, composition C1. Silicalite-1 did not form in C1 over one year at room temperature, but instead a dense silica phase was observed (see Supplementary Information, Fig. S7). Examination of these crystals by TEM shows that they have a compact, single-crystalline morphology with no indication of aggregative growth. As mentioned previously, it appears that silicalite-1 is able to exist in C1 from a solubility standpoint. Failure to generate silicalite-1 at C1 may be attributed to slow nucleation due to the absence of closely associated TPA and silicate species. As a result, nucleation of dense silica from monomeric silicate species is favoured.

Comparing experimental results at C1 and C3, it seems that the precursor nanoparticles, which bring silica and TPA together, are necessary for nucleation. Experimental results at C8 show that the presence of nanoparticles is not a sufficient condition for silicalite-1 nucleation and growth. At C8, although precursor nanoparticles are present, silicalite-1 crystals do not form within a year. Instead, dense silica is formed. This indicates that, although the nanoparticle concentration is larger at C8 than at C3, the C8 nanoparticles evolve much more slowly (if at all) to silicalite-1. A major difference between C3 and C8 is the ratio of TPA to silica, and thus of TPA per nanoparticle. Specifically, the ratio of TPA per nanoparticle for C8 is less than that for C3. The reduced rate of evolution observed for C8 may be attributed to this lower concentration of TPA available per nanoparticle. Therefore, a picture emerges in which the nanoparticles, despite their narrow size distribution, are a diverse population evolving in composition. In this respect, the precursor nanoparticles follow an amorphous-to-crystalline evolution similar to that observed when starting from concentrated mixtures that include visible amorphous precipitates[35].

The first experimental evidence for a distributed and evolving precursor nanoparticle population is demonstrated here by *in situ* AFM. Mica surfaces were first etched with hydrofluoric acid (HF) to create 1.1-nm steps on the mica surface, features that could then be used as an internal calibration standard for accurately measuring the dimensions of deposited precursor nanoparticles by AFM. The mica surfaces were imaged while immersed in C3 that had been aged for different periods of time (0 days to 12 months). Control experiments indicated that no changes to the mica surface occur within the timescale of the experiment (~1 h), when mica is immersed in a TPAOH solution. Images were collected 5–90 min

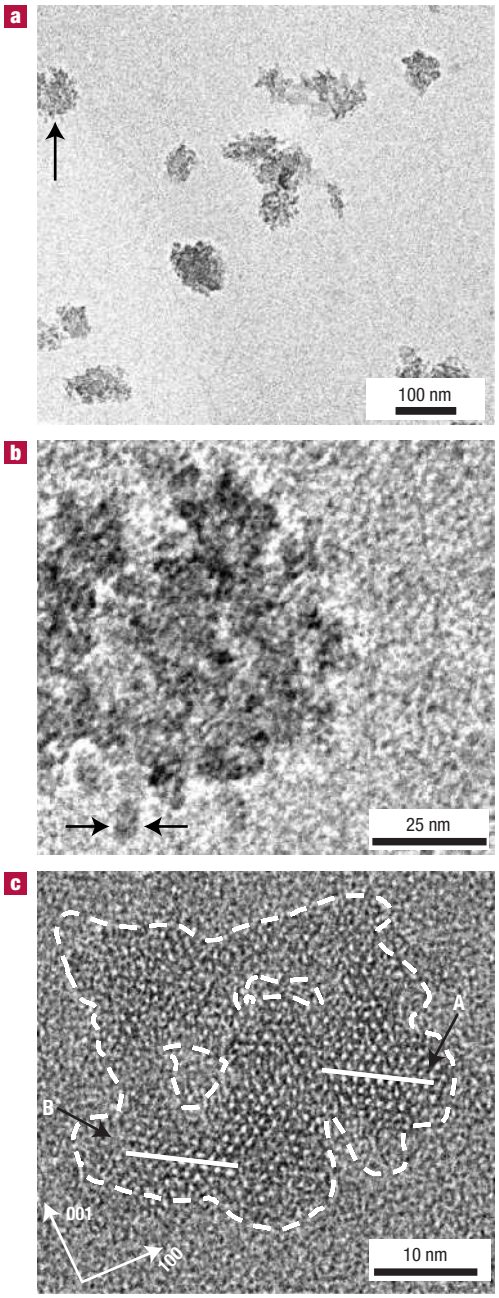

Figure 4 TEM characterization of TPA-silicalite-1 crystals present in C3 after 305 days of ageing (crystal yield less than 5%). a, Lower-magnification images show a crystal population with radii up to 50 nm and a broad size distribution. **b**, Higher magnification of the crystal indicated in **a** shows an aggregate-like morphology with domains of the order of 5 nm (also see Supplementary Information, Fig. S5). **c**, Representative HRTEM image of TPA-silicalite-1 shows that the aggregate-like particle is a single crystal with small in-plane misorientations. This image is a view down the straight channels of the framework, that is, ⟨010⟩ zone-axis (also see Supplementary Information, Fig. S6).

after the introduction of C3 to the AFM liquid cell. Figure 5 shows two representative images obtained in contact mode with an unmodified silicon nitride tip 60 min after the introduction of C3 to the AFM liquid cell. Figure 5a shows a height image for fresh C3 and Fig. 5c shows a height image for mica in contact with 12-month-aged C3 from which the zeolite crystals have been removed by ultracentrifugation (examination by SAXS indicated a single-particle population with a size of 5 nm). These images (Fig. 5a,c) show that for aged C3, bright features appear on the steps of etched mica surfaces in addition to the 1.1-nm mica steps. Such bright features (other than the mica steps) are not present in images taken from mica immersed in fresh C3. This difference is more clearly shown by the line profiles shown in Fig. 5b,d. The heights of the bright features detected on mica immersed in the 12-month aged C3 ranged from 4 to 5 nm, consistent with the estimated size of precursor nanoparticles from SAXS and cryo-TEM. The majority of the particles are present at the mica steps, an observation that can be attributed to particles being pushed by the tip during imaging or to preferential adsorption at steps. This finding indicates nanoparticle evolution with respect to colloidal stability and to affinity for attachment to the mica surface.

Additional imaging experiments were carried out using OH-terminated tips in tapping mode in an effort to alter the tip–nanoparticle interaction. In these experiments, the mica steps, although visible, were not always accurately resolved, and as a result the experiments were not used to provide accurate size determination. However, they provide evidence to support the hypothesis made above that nanoparticles are pushed on the mica surface by the unmodified AFM tip during contact-mode imaging. The tip–nanoparticle interaction is apparently reduced when OH-terminated tips are used and as a result, nanoparticles were detected on both the mica steps and terraces. The nanoparticles appear as bright dots and lines (see Supplementary Information, Fig. S8), where the lines can be interpreted as nanoparticles pushed during imaging. AFM height images indicate a size of 2.5–4.0 nm, values that are less than those detected using unmodified tips in contact mode and those measured by SAXS and cryo-TEM. This difference is not surprising considering the limited accuracy by which the mica step heights could be determined in tapping mode. Figure 5e shows the concentration of features (dots and lines) with heights greater than 2.5 nm as a function of time in contact with three C3 mixtures: fresh, 2-month aged, and 12-month aged. This plot provides additional evidence that ageing C3 leads to an increase in nanoparticle attachment to mica.

Although precursor nanoparticle dragging at the mica surface introduced quantitative uncertainties regarding the surface concentration and location of precursor nanoparticles on the mica surface, the AFM results from both modified and unmodified tips clearly indicate that there is a qualitative difference between fresh and aged precursor nanoparticles with respect to their propensity for attachment to the mica surface. This finding indicates precursor nanoparticle evolution resulting in differences in colloidal stability for a fraction of the nanoparticles.

In summary, the TEM data show strong evidence that there is an aggregative growth mechanism dominating early stages of crystal growth. *In situ* SAXS and cryo-TEM indicate that there is a period of time during which the precursor nanoparticles remain at a constant size, whereas *in situ* AFM provides evidence that they continue to evolve with respect to their colloidal stability and propensity for attachment to a mica surface. SAXS, XRD and TEM show that silicalite-1 crystals, even at crystal yields as low as 5%, reach radii of the order of 50 nm, comparable to those reached at high yields.

A kinetic mechanism was formulated that can account for the above findings. The proposed mechanism for the evolution of precursor nanoparticles to silicalite-1 crystals is shown schematically in Fig. 6a. A mathematical model was developed on the basis of this mechanism and mass-action kinetics (see the Methods section for equations). In the model, the precursor nanoparticles that do not contribute to aggregative growth are

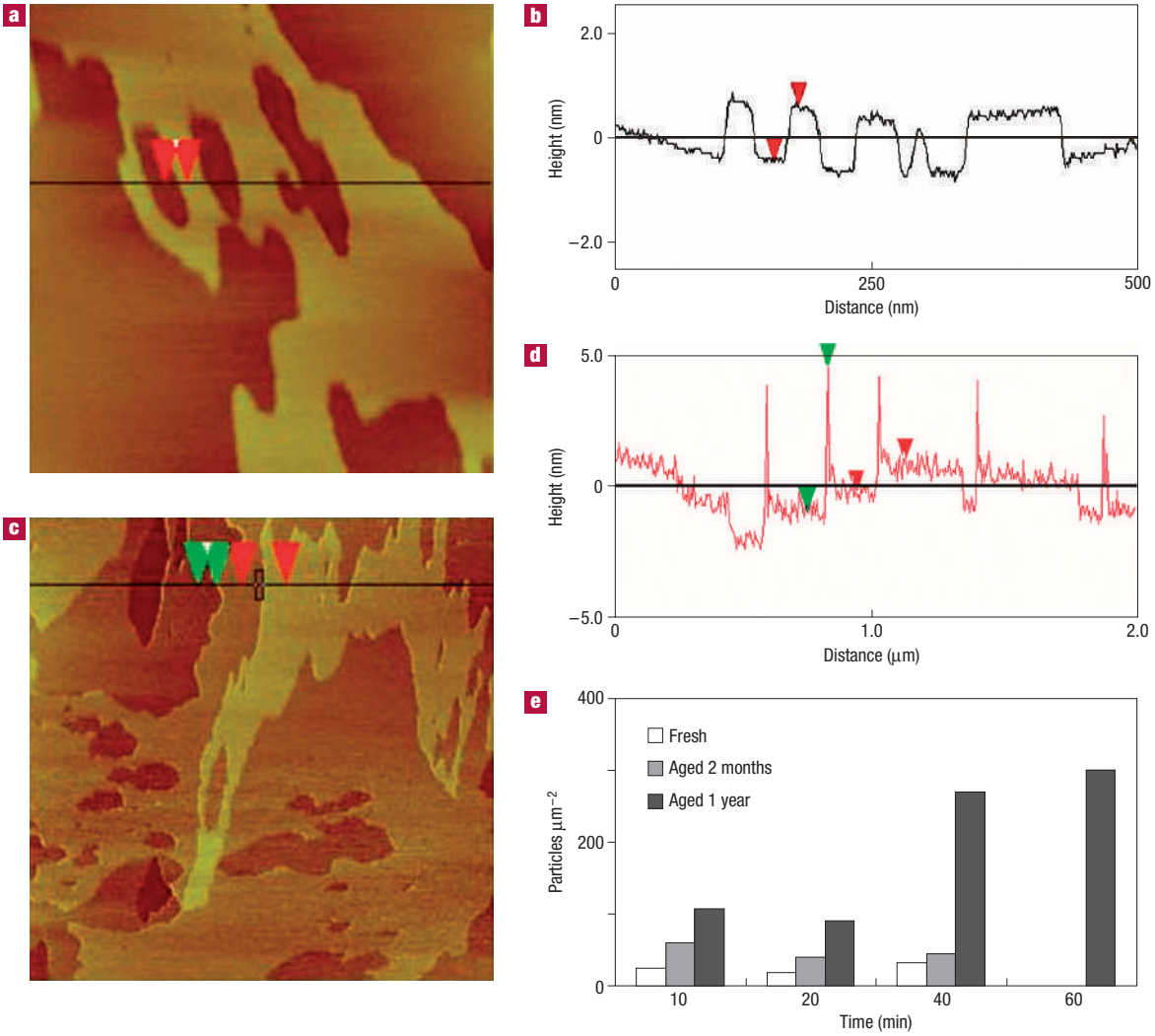

Figure 5 Attachment of precursor nanoparticles on mica surfaces by liquid phase *in situ* AFM imaging. a, Mica surface imaged using a silicon nitride tip in contact mode 60 min after the introduction of fresh C3; image is 0.5 μm × 0.5 μm. **b**, The corresponding height image of **a** only shows the 1.1-nm steps of HF-etched mica. The red arrows mark a typical step in **a** and **b**. **c**, Mica surface imaged using a silicon nitride tip in contact mode 60 min after the introduction of 350-day aged C3. The bright spots concentrated at the mica steps indicate deposited particles. **d**, The corresponding height image of **c** shows, in addition to the 1.1-nm steps of HF-etched mica (see red arrows for a typical step), features 4–5 nm in height (see green arrows). These features are attributed to precursor nanoparticles deposited on mica and pushed to the mica steps by the AFM tip during imaging. **e**, Concentration of features, imaged by tapping-mode AFM and OH-modified tips, with sizes larger than 2.5 nm on mica surfaces as a function of time in contact with the indicated C3 mixture (fresh, 2-month aged, and 12-month aged). See Supplementary Information, Fig. S8 for a sample image obtained using OH-functionalized tips.

depicted as particles A. They can gradually evolve through m intermediates (B_1 to B_m) to silicalite-1 nuclei, C_1. Particles A, along with the intermediate particles, can dissolve with a rate that is fast compared with the evolution process. We consider that particles A do not have the zeolite structure (they are disordered (silica) core-(TPA) shell particles) and they do not contribute substantially to aggregation. This lack of participation in aggregation can be attributed to the following two characteristics: the A particles have relatively fast dissolution dynamics and/or they have increased colloidal stability compared with zeolite-like particles. The increased colloidal stability may be due to negative surface charge and to steric stabilization by adsorbed structure-directing agent (SDA), as was suggested previously[4,13].

Precursor nanoparticles B_1 to B_m have reduced colloidal stability and/or dissolution rate, and their structure is increasingly similar to zeolite particles. These intermediate particles, although not yet silicalite-1 nuclei, can contribute to crystal growth by attachment. Nuclei and growing crystals are denoted as C_1 to C_n. Here, to emphasize the essential novel elements of the proposed mechanism, we neglect zeolite dissolution, growth by crystal–crystal aggregation, and Ostwald ripening involving monomeric or oligomeric species.

The mathematical model has the following parameters: the initial number of precursor nanoparticles (n_{A_0}), the forward and backward effective kinetic constants (k_+ and k_-) for nanoparticle evolution, the number of evolution steps (m), and the precursor nanoparticle crystal coalescence rate constant (β_{ij}). The number of nanoparticles is estimated using absolute SAXS intensities and the procedure of Rimer *et al.*[4,36] that assumes a TPA-free silica core. At composition C3, $n_{A_0} \cong 10^{17}$ particles cm^{-3} in

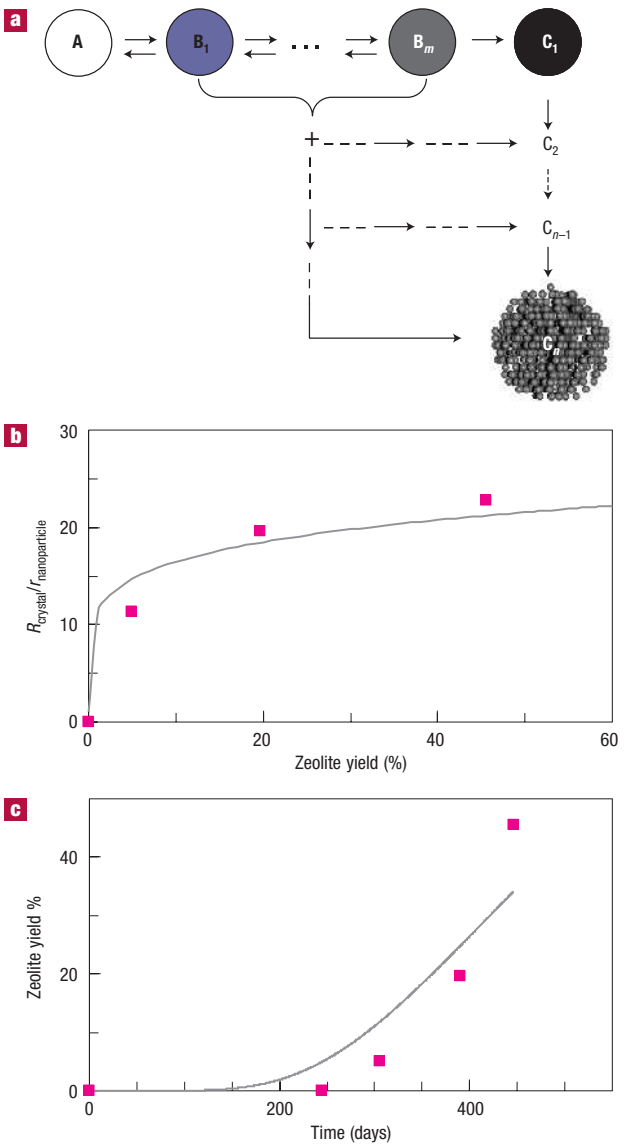

Figure 6 Simulation data from mathematical model of nanoparticle ageing and growth mechanism. a, Schematic illustration of the mechanism proposed for nanoparticle evolution and crystal growth by aggregation. **b**, Crystal size as a function of the per-cent zeolite yield. The data points are from the experiments shown in Fig. 3, and the solid line is fitted using the quasi-steady-state model (see Methods, equation (D)) with $b/K^{(m-1)} = 10^8$. **c**, Per-cent zeolite yield as a function of time. The data points are from experiments and the solid line is fitted from the full model (see Methods, equations (A)–(C)) with parameters $k_+ = 9.01 \times 10^{-4}$ h^{-1}, $k_- = 2.55 \times 10^{-3}$ h^{-1}, $\beta = 2.12 \times 10^{-26}$ m^3 s^{-1}, $n_{A_0} = 10^{17}$ particles cm^{-3}, and $m = 10$.

agreement with a previously reported estimation[14]. This estimation is also in close agreement with the concentration of precursor nanoparticles estimated using the cryo-TEM images by assuming a sample thickness in the range of 100–500 nm ($n_{A_0} \cong 1.2$–6.0×10^{17} particles cm^{-3}). Accordingly, approximately 200–250 Si atoms are estimated to be present in a nanoparticle. The number of evolution steps (m) is set to ten because a precursor nanoparticle of 200–250 Si atoms will have to incorporate 8–10 TPA cations when transformed to the silicalite-1 structure.

In the model, it is assumed that the rate constant for coalescence, β_{ij}, is a constant, independent of i and j and will be referred to as β from here on. The assumption of β_{ij} independent of j (the size of the silicalite-1 crystal) may appear to be a drastic simplification at first, because as silicalite-1 crystals grow, the addition of nanoparticles by attachment may be affected due to changes in diffusivity, attachment area, and colloidal stability ratio. More specifically, an expression for β_{ij} for spherical crystals and particles is as follows[37]

$$\beta_{ij} = \frac{2kT}{3\mu}(r_i + R_j)\left(\frac{1}{r_i} + \frac{1}{R_j}\right)\frac{1}{W_{ij}}$$

with r_i and R_j being the radii of particles and crystals, respectively, μ being the solution viscosity, kT being the product of Boltzmann's constant and absolute temperature, and W_{ij} being the stability ratio that can be estimated from DLVO theory. For radii within the range 2.5–30 nm, the quantity $(r_i + R_j)\left[(1/r_i) + (1/R_j)\right]$ varies from 4 to 14 and therefore, to a first approximation, it can be considered as constant. The stability ratio is a strongly decreasing function of r_i and R_j for compact particles with smooth surfaces. However, in the case at hand, for early stages of growth, the zeolite crystals have very rough surfaces with surface roughness of the order of the precursor nanoparticles (about 5 nm), as was shown in the TEM images. The 5-nm roughness of the silicalite-1 crystals during the initial stages of growth justifies the approximation of W_{ij} being independent of the silicalite-1 crystal size in our model. At later stages of growth, when zeolite crystal facets develop, this approximation will lead to an overestimation of precursor nanoparticle rate of attachment. Although the assumption of β_{ij} being independent of j can be justified on the basis of crystal surface roughness, the independence of β_{ij} on i (that is, the stage of evolution of precursor nanoparticles) is a drastic one. On the basis of the AFM evidence shown above, as precursor nanoparticles evolve, their colloidal stability will decrease leading to increased β_{ij} with increasing i. However, as will be shown elsewhere, simulations indicate that changes in β_{ij} with increasing i do not significantly affect the yield versus time predictions of the model, but mainly affect the sharpness of the crystal size distribution. Therefore, the assumption of constant β_{ij} is considered an acceptable simplification that permits conceptualization of the mechanism introduced here.

The stability ratio for two 5-nm particles with a surface potential of −45 mV was calculated from a DLVO model[14] to be 5.18×10^8. Given this value of the stability ratio, β was calculated to be 2.12×10^{-26} m^3 s^{-1}. Once β, n_{A_0}, and m are fixed, two parameters in the model are left to be specified, k_+ and k_-. Although these parameters may be a function of m, here we consider them to be constants, irrespective of the evolution step (this assumption can be removed providing added flexibility to better fit the experimental data). They are specified by fitting the model to experimental data for particle size as a function of crystal yield (see Fig. 6b) and crystal yield as a function of time (see Fig. 6c) (see the Methods section for a detailed description of the fitting procedure). With the mechanism described in Fig. 6a, a good fit to the experimental data is obtained.

In summary, the simulation results indicate that the experimental data can be explained by a mechanism where the precursor nanoparticles evolve to zeolite crystals through several intermediate states that can contribute to aggregative growth. According to the proposed mechanism, the concentration of each intermediate species is significantly lower than the initial concentration of fresh particles. Moreover, the concentration of the intermediates decreases significantly as the intermediates progress towards silicalite-1.

Owing to the decrease in concentration of the intermediate species as they progress further towards becoming silicalite-1, and the assumed size-independent coalescence constant, the B_1 particles, which are at the earliest stage of evolution, are the most important contributors to aggregative growth. In fact, similar yield predictions are obtained by neglecting the contribution to crystal growth by nanoparticles B_2 to B_m. At the expense of introducing additional parameters, the model can be modified to account for age- and size-dependent evolution and coalescence, providing an improved fit to the experimental data.

The indispensable element of the proposed model is that the evolving population of silica nanoparticles, although homogeneous in size and shape, exhibits functional diversity towards aggregative crystal growth due to structural differentiation among the nanoparticles. The proposal put forward here, that the precursor nanoparticles are distributed in structure, may reconcile previous contradicting views that were expressed on the basis of interpreting data from this system considering a homogeneous nanoparticle population (for example, nanoslabs, amorphous core–shell ellipsoids). Moreover, the demonstration of distinct colloidal stability characteristics among the evolving metastable nanoparticles may lead to procedures for isolating and using the small fraction of progressively zeolite-like precursor nanoparticles as building blocks for novel materials—a highly sought after, but still elusive goal in the area of hydrothermal zeolite synthesis.

METHODS

SYNTHESIS

TPA–silica mixtures were prepared from TPAOH (1.0 M Aldrich) and TEOS (98% Aldrich), stirred for ~24 h and then poured into 4 oz. Teflon-coated plastic bottles (Fisher Scientific) for ageing. ~2 ml aliquots were removed monthly for characterization. Mixtures were not stirred during ageing, but rotated immediately before the removal of a sample. The lab temperature was recorded throughout the experiment (see Supplementary Information, Fig. S9).

SAXS

Samples were placed in a vacuum-tight 1-mm quartz capillary, and scattering was measured using Cu Kα radiation and the SAXSess SAXS instrument (Anton Paar) at room temperature (25 °C). SAXS patterns were normalized with respect to incident beam intensity, and scattering from water was subtracted as background. The experimental data was corrected for instrumental broadening caused by the line-collimated incident beam. The GIFT software[19] was used to analyse the SAXS data. PDDF were obtained by fitting the background subtracted, absolute intensity SAXS patterns and then using the indirect Fourier transform technique[18,38]. Experimental PDDF were fitted with a Schultz distribution of spheres using the method described in the Supplementary Information.

SANS

SANS was measured at the National Institute of Standards and Technology (NIST) in Gaithersburg, Maryland, on the NG7 30-m instrument, using quartz cells with a 4-mm path length. Two sample-to-detector distances (3 and 13 m) and a constant neutron wavelength of 6 Å were used to obtain scattering profiles from $q = 0.05$ to 1.4 nm^{-1}. NIST provided software for reduction of the experimental data[39]. This data was then corrected for background scattering and entered into the GIFT software to obtain PDDF.

CRYO-TEM

Specimens were prepared by transferring a small drop of the liquid to a holey carbon-film-coated TEM grid (Ted Pella). The droplet was thinned to a film by blotting with filter paper from the backside of the grid, and the specimen was immediately plunged into liquid ethane. Details of this procedure are given by Talmon[40]. Resulting specimens were transferred to a Gatan 613.DH Cooling Holder (−180 °C) and imaged at 120 kV using a JEOL 1210 TEM equipped with a Gatan 724 charge-coupled device camera.

TWO-STEP DIALYSIS

A two-step dialysis procedure of the aged mixtures allowed separation of the crystals from the nanoparticles, dissolved silica and TPA ions. First, the aged mixture was transferred to a rinsed dialysis tube (Spectra Por 3, Spectrum Laboratories). The tube was then sealed closed and placed in a 1 l polypropylene beaker containing 6 ml 1.0 M TPAOH and 1 l water (pH ~ 11.5). The TPA/water solution was stirred slowly, allowing the dialysis tube to rotate. After ~24 h of stirring, the dialysis tube was placed in another beaker only containing water. The tube was rotated in the water by magnetic stirring, and the pH of the mixture inside the dialysis tube was reduced. The water was exchanged when the pH of the water outside the tube increased above ~8.5. After a total of ~48 h of stirring in water, the water pH stabilized at ~pH8, signifying that the dialysis was complete.

TEM, XRD, SEM, DLS

A TEM grid was prepared for each dialysed sample by diluting a small amount of suspension in ethanol, and then placing a droplet onto a holey carbon-coated copper grid. Specimens were allowed to air-dry, and were then imaged at 300 kV using an FEI Tecnai F30 HRTEM operated at 300 kV and equipped with a charge-coupled device camera. Crystallinity of the particles was verified using a PANalytical X'Pert PRO X-ray diffractometer equipped with an X'Celerator detector and cobalt source ($\lambda = 0.1789$ nm). SEM was carried out using a JEOL 6500 SEM, equipped with a field emission gun operated at 5.0 kV. DLS measurements were made using a ZetaPALS instrument (Brookhaven Instruments), and the particle size was estimated using software provided by Brookhaven Instruments.

AFM

For AFM, muscovite mica was etched in concentrated HF for 4 h to generate the ~1-nm steps used as an internal standard[41]. A Nanoscope III AFM was used to image the etched mica surfaces. Imaging was first done in water to ensure that the surfaces and the whole system were clean, and that there was no adsorption of small particles. Then images of the etched mica were taken in fresh and aged C3 using contact and tapping modes with unmodified or OH-functionalized silicon nitride tips. AFM tips were coated with a layer of gold, and then functionalized by soaking in a 10^{-3} M $HS(CH_2)_{10}CH_2OH$ thiol solution for 18 h (refs 42,43). The line-profile analysis was carried out using the software Nanoscope III 5.12r3.

MATHEMATICAL MODEL

In the model, precursor nanoparticle evolution is considered a reversible process (due to dynamic nanoparticle dissolution and reformation). All of the forward and reverse reactions are considered first-order with equal rate constants, k_+ and k_- correspondingly. The attachment of B_i particles to silicalite-1 nuclei and growing crystals C_j is considered a second-order reaction with rate constant β_{ij}. Here n_A and n_{B_i} are the number per unit volume of particles A or B_i, and n_{A_0} is the initial number of precursor nanoparticles, estimated to be ~10^{17} particles cm^{-3} for composition C3. The model consists of the following set of ordinary differential equations for nanoparticle evolution and crystal growth

$$\text{A particles}\ \left\{ \frac{dn_A}{dt} = -k_+ n_A + k_- n_{B_1} \right. \tag{A}$$

$$\text{B particles}\ \begin{cases} \frac{dn_{B_1}}{dt} = k_+ n_A - k_- n_{B_1} - k_+ n_{B_1} + k_- n_{B_2} - n_{B_1} \sum_{i=1}^{\infty} n_{C_i} \beta_{1i} \\ \frac{dn_{B_2}}{dt} = k_+ n_{B_1} - k_- n_{B_2} - k_+ n_{B_2} + k_- n_{B_3} - n_{B_2} \sum_{i=1}^{\infty} n_{C_i} \beta_{2i} \\ . \\ . \\ . \\ \frac{dn_{B_{m-1}}}{dt} = k_+ n_{B_{m-2}} - k_- n_{B_{m-1}} - k_+ n_{B_{m-1}} + k_- n_{B_m} \\ - n_{B_{m-1}} \sum_{i=1}^{\infty} n_{C_i} \beta_{(m-1)i} \\ \frac{dn_{B_m}}{dt} = k_+ n_{B_{m-1}} - k_- n_{B_m} - k_+ n_{B_m} - n_{B_m} \sum_{i=1}^{\infty} n_{C_i} \beta_{mi} \end{cases} \tag{B}$$

$$\text{crystals}\begin{cases}\frac{dn_{C_1}}{dt} = n_{B_m} - \sum_{j=1}^{m} n_{B_j} n_{C_1} \beta_{j1} \\ \frac{dn_{C_2}}{dt} = \sum_{j=1}^{m} n_{B_j}\left(n_{C_1}\beta_{j1} - n_{C_2}\beta_{j2}\right) \\ \cdot \\ \cdot \\ \cdot \\ \frac{dn_{C_k}}{dt} = \sum_{j=1}^{m} n_{B_j}\left(n_{C_{(k-1)}}\beta_{j(k-1)} - n_{C_k}\beta_{jk}\right) \\ \cdot \\ \cdot \\ \cdot \end{cases} \quad (C)$$

In the simulations presented here, it is assumed that $\beta_{11} \cong \beta_{12} \cong \cdots \cong \beta_{1k} = \beta$. From this set of equations, we also get

$$\frac{d\left(\sum_{i=1}^{\infty} n_{C_i}\right)}{dt} \cong n_{B_m}.$$

To obtain the parameters k_+ and k_- the following procedure was used. A quasi-steady-state solution of the model was obtained, which, among other approximate predictions, provided the following relationship between dimensionless crystal size measured by SAXS and zeolite yield:

$$\left(\frac{R_{SAXS}}{r}\right) = (i_{SAXS})^{(1/3)} \cong \left(1 + 2\frac{b}{K^{(m-1)}}(\%\ \text{zeolite yield})\right)^{(1/6)}, \quad (D)$$

where $b = \beta n_{A_0}/k_+$ and $K = k_+/k_-$. The experimental data of the particle size observed in SAXS normalized by the size of precursor nanoparticles was plotted versus (crystal yield)$^{(1/6)}$ to give a linear plot. From the slope of the fit line, the parameter $2b/K^{(m-1)}$, where $b = \beta n_{A_0}/k_+$ and $K = k_+/k_-$, was estimated to be 2×10^8. As m was set to 10 and β was calculated from DLVO theory, the slope provided a relationship between k_+ and k_-. The experimental crystal yield was then plotted as a function of time, the full model (non-quasi-steady-state version) was run, and the simulation was fitted to the experimental delay time for the appearance of silicalite-1 by adjusting k_+ and k_- while preserving the value of $b/K^{(m-1)} = 10^8$.

Received 12 December 2005; accepted 24 March 2006; published 16 April 2006.

References

1. Corma, A. & Davis, M. E. Issues in the synthesis of crystalline molecular sieves: Towards the crystallization of low framework-density structures. *ChemPhysChem* **5,** 304–313 (2004).
2. Yang, S., Navrotsky, A., Wesolowski, D. & Pople, J. Study on synthesis of TPA-silicalite-1 from initially clear solutions of various base concentrations by in situ calorimetry, potentiometry, and SAXS. *Chem. Mater.* **16,** 210–219 (2004).
3. Schoeman, B. & Regev, O. A study of the initial stage in the crystallization of TPA-silicalite-1. *Zeolites* **17,** 447–456 (1996).
4. Fedeyko, J., Rimer, J., Lobo, R. & Vlachos, D. Spontaneous formation of silica nanoparticles in basic solutions of small tetraalkylammonium cations. *J. Phys. Chem. B* **108,** 12271–12275 (2004).
5. Mintova, S., Olson, N., Senker, J. & Bein, T. Mechanism of the transformation of silica precursor solutions into Si-MFI zeolite. *Angew. Chem. Int. Edn* **41,** 2558–2561 (2002).
6. Cheng, C.-H. & Shantz, D. F. Nanoparticle formation and zeolite growth in TEOS/organocation/water solutions. *J. Phys. Chem. B* **109,** 7266–7274 (2005).
7. de Moor, P. P., Beelen, T. & van Santen, R. In situ observation of nucleation and crystal growth in zeolite synthesis. A small-angle X-ray scattering investigation on Si-TPA-MFI. *J. Phys. Chem. B* **103,** 1639–1650 (1999).
8. Houssin, C. *et al.* Combined in situ Si NMR and small-angle X-ray scattering study of precursors in MFI zeolite formation from silicic acid in TPAOH solutions. *Phys. Chem. Chem. Phys.* **5,** 3518–3524 (2003).
9. Cheng, C. H. & Shantz, D. Silicalite-1 growth from clear solution: effect of the structure-directing agent on growth kinetics. *J. Phys. Chem. B* **109,** 13912–13920 (2005).
10. Twomey, T. A. M., Mackay, M., Kuipers, H. P. C. E. & Thompson, R. W. In situ observation of silicalite nucleation and growth: A light-scattering study. *Zeolites* **14,** 162–168 (1994).
11. Choi, J., Ghosh, S., Lai, Z. & Tsapatsis, M. Uniformly a-oriented MFI zeolite films by secondary growth. *Angew. Chem. Int. Edn* **45,** 1154–1158 (2006).
12. Drews, T. O. & Tsapatsis, M. Progress in manipulating zeolite morphology and related applications. *Curr. Opin. Colloid Interface Sci.* **10,** 233–238 (2005).
13. Schoeman, B. J. Analysis of the nucleation and growth of TPA-silicalite-1 at elevated temperatures with the emphasis on colloidal stability. *Micropor. Mesopor. Mater.* **22,** 9–22 (1998).
14. Nikolakis, V., Kokkoli, E., Tirrell, M., Tsapatsis, M. & Vlachos, D. Zeolite growth by addition of subcolloidal particles: modeling and experimental validation. *Chem. Mater.* **12,** 845–853 (2000).
15. Kirschhock, C. E. A. *et al.* Zeosil nanoslabs: building blocks in $n Pr_4N^+$-mediated synthesis of MFI zeolite. *Angew. Chem. Int. Edn* **40,** 2637–2640 (2001).
16. Corkery, R. W. & Ninham, B. W. Low-temperature synthesis and characterization of a stable colloidal TPA-silicalite-1 suspension. *Zeolites* **18,** 379–386 (1997).
17. deMoor, P.-P. E. A., Beelen, T. P. M., van Santen, R. A., Beck, L. W. & Davis, M. E. Si-MFI crystallization using a "Dimer" and "Trimer" of TPA studied with small-angle X-ray scattering. *J. Phys. Chem. B* **104,** 7600–7611 (2000).
18. Glatter, O. The interpretation of real-space information from small-angle scattering experiments. *J. Appl. Crystallogr.* **12,** 166–175 (1979).
19. Bergmann, A., Fritz, G. & Glatter, O. Solving the generalized indirect Fourier transformation (GIFT) by Boltzmann simplex simulated annealing (BSSA). *J. Appl. Crystallogr.* **33,** 1212–1216 (2000).
20. Gilbert, B., Huang, F., Zhang, H., Waychunas, G. A. & Banfield, J. F. Nanoparticles: strained and stiff. *Science* **305,** 651–654 (2004).
21. Gawrys, K. L. & Kilpatrick, P. K. Asphaltenic aggregates are polydisperse oblate cylinders. *J. Colloid Interface Sci.* **288,** 325–334 (2005).
22. Orthaber, D., Bergmann, A. & Glatter, O. SAXS experiments on absolute scale with Kratky systems using water as a secondary standard. *J. Appl. Crystallogr.* **33,** 218–225 (2000).
23. Jorge, M., Auerbach, S. M. & Monson, P. A. Modeling spontaneous formation of precursor nanoparticles in clear-solution zeolite synthesis. *J. Am. Chem. Soc.* **127,** 14388–14400 (2005).
24. Burleson, D. J. & Penn, R. L. Two step growth of goethite from ferrihydrite. *Langmuir* **22,** 402–409 (2006).
25. Buyanov, R. & Krivoruchko, O. Development of a theory of crystallization of difficultly soluble metal hydroxides and of scientific bases for the preparation of catalysts from substances of this class. *Kinetics Catal.* **17,** 666–675 (1976).
26. Buyanov, R., Krivoruchko, O. & Ryzhak, I. Mechanism of the nucleation and growth of crystals of iron hydroxide and iron oxide in mother liquors. *Kinetics Catal.* **13,** 470–478 (1972).
27. Mackenzie, R. C. & Meldau, R. The ageing of sesquioxide gels. I. Iron oxide gels. *Mineral Mag.* **32,** 153–165 (1959).
28. Navrotsky, A. Energetic clues to pathways to biomineralization: precursors, clusters, and nanoparticles. *Proc. Natl Acad. Sci.* **101,** 12096–12101 (2004).
29. Penn, R. Kinetics of oriented aggregation. *J. Phys. Chem. B* **108,** 12707–12712 (2004).
30. Penn, R. L. & Banfield, J. F. Imperfect oriented attachment: dislocation generation in defect-free nanocrystals. *Science* **281,** 969–971 (1998).
31. Mintova, S., Olson, N. H., Valtchev, V. & Bein, T. Mechanism of zeolite a nanocrystal growth from colloids at room temperature. *Science* **283,** 958–960 (1999).
32. Mintova, S., Olson, N. H. & Bein, T. Electron microscopy reveals the nucleation mechanism of zeolite Y from precursor colloids. *Angew. Chem. Int. Edn* **38,** 3201–3204 (1999).
33. Bonilla, G. *et al.* Zeolite (MFI) crystal morphology control using organic structure-directing agents. *Chem. Mater.* **16,** 5697–5705 (2004).
34. Wollast, R. & Garrels, R. Diffusion coefficient of silica in seawater. *Nature* **229,** 94 (1971).
35. Corma, A. & Diaz-Cabanas, M. J. Amorphous microporous molecular sieves with different pore dimensions and topologies: synthesis, characterization, and catalytic activity. *Micropor. Mesopor. Mater.* **89,** 39–46 (2006).
36. Rimer, J., Vlachos, D. & Lobo, R. Evolution of self-assembled silica-tetrapropylammonium nanoparticles at elevated temperatures. *J. Phys. Chem. B* **109,** 12762–12771 (2005).
37. Van Hyning, D. L., Klemperer, W. G. & Zukoski, C. F. Silver nanoparticle formation: Predictions and verification of the aggregative growth model. *Langmuir* **17,** 3128–3135 (2001).
38. Glatter, O. A new method for the evaluation of small-angle scattering data. *J. Appl. Crystallogr.* **10,** 415–421 (1977).
39. NIST SANS Data Reduction. <http://www.ncnr.nist.gov/programs/sans/data/data_red.html>.
40. Talmon, Y. in *In Modern Characterization Methods of Surfactant Systems* (ed. Binks, B. P.) (Marcel Dekker, New York, 1999).
41. Nagahara, L. A., Hashimoto, K., Fujishima, A., Snowden-Ifft, D. & Price, P. B. Mica etch pits as a height calibration source for atomic force microscopy. *J. Vac. Sci. Technol. B* **12,** 1694–1697 (1994).
42. Ulman, A. *et al.* Concentration-driven surface transition in the wetting of mixed alkanethiol monolayers on gold. *J. Am. Chem. Soc.* **113,** 1499–1506 (1991).
43. Evans, S. D., Sharma, R. & Ulman, A. Contact angle stability: reorganization of monolayer surfaces? *Langmuir* **7,** 156–161 (1991).

Acknowledgements

Financial support for this work was provided by NSF (NIRT CTS-0103010 and CTS-05 22518). The HRTEM work was supported in part by NSF-MRI EAR-0320641 and the MRSEC Program of NSF under Award Number DMR-0212302. M.K. acknowledges support from NSF (DMS-041386). Characterization was carried out at the Minnesota Characterization Facility, which receives support from NSF through the National Nanotechnology Infrastructure Network. Numerical simulations were carried out using the facilities of the Supercomputing Institute for Digital Simulation and Advanced Computation at the University of Minnesota. We thank A. Parr for lending us the SAXSess instrument; F. S. Bates for providing access to SANS analysis at NIST and for helpful discussions; and R. Bedard, D. G. Vlachos, V. Nikolakis, R. F. Lobo and V. Hatzimanikatis for input at various stages of this work. Correspondence and requests for materials should be addressed to M.T.
Supplementary Information accompanies this paper on www.nature.com/naturematerials.

Competing financial interests

The authors declare that they have no competing financial interests.